

TROPPO - A Tropospheric Propagation Simulator

Technical Report 2004/161

Carlo Kopp,
Email: carlo@csse.monash.edu.au

C.S. Wallace *FACM, FACS*

November 17, 2004

Contents

1	Introduction	3
2	Propagation Loss Models	4
3	The Atmospheric Model	4
4	The Water Vapour Absorption Model	6
5	The Oxygen Absorption Model	8
6	The Lens Effect Loss Model	10
7	The Cloud Scattering Loss Model	13
8	The Rain Scattering Loss Model	14
9	The Refractive Model	15
10	Path Loss, SNR and Capacity	16
11	Combined Simulations	19
12	Conclusions	19
13	Background	20

1 Introduction

An interesting problem which frequently arises in microwave communication and radar engineering is the calculation of microwave propagation losses through the troposphere and lower stratosphere. A wealth of detailed literature and software tools exists for calculating losses in propagation geometries which are characteristic of terrestrial satellite and point to point links, and surface based radar installations. The more general case is less frequently addressed. Given the inhomogeneous and widely variable physical properties of the atmosphere, the use of simplified models for solving the general propagation problem will mostly yield unsatisfactory results.

The growth in Low Earth Orbit (LEO) communication satellite usage, the increasing popularity of directional and non-directional airborne datalinks to support Uninhabited Aerial Vehicles (UAV) and general military air operations, requires the solution of the general propagation problem for arbitrary station altitudes in the troposphere and lower stratosphere.

This paper discusses the design and implementation of the TROPospheric PrOpagation simulator tool (TROPPO), which implements a general propagation model for stations with arbitrary altitudes up to the lower stratosphere. TROPPO solves the nonlinear refractive ODE boundary value problem, using two algorithms, and implements several models for variations of pressure and water vapour density with altitude, water vapour and oxygen resonances, cloud droplet scattering, rain absorption and lense effect loss, for a wide range of configurable initial conditions. The Friis pathlength loss is modelled and receiver SNR and link Shannon capacity are calculated.

The need for a propagation simulator capable of handling the general case became evident during work on a research project dealing with the achievable performance limits of mobile communications employing directional microwave beams. A tool was required with the capability to model specific scenarios with reasonable accuracy, and the tool would need to be adaptable for use in other simulations as a C-language library.

Much of the literature on atmospheric propagation effects, such as the NASA Satellite Systems Design Handbooks by Ippolito [1] and Flock [2], and radar propagation texts by Blake [3], [4] and Meeks [5], provides well proven and widely used models for specific propagation impairments. This literature was used as a basis for the models implemented in the TROPPO simulator. The use of commonly accepted models was specifically intended to allow easy calibration and testing of the implementation against a known and previously tested benchmark.

The TROPPO simulator was designed from the outset to be modular, to allow the incorporation of alternative models for specific propagation effects. Provisions were made for selection of some alternative models in the code, but these have not been implemented as yet since the existing model set proved adequate for the intended purpose.

From a functional perspective, the TROPPO simulator has two primary operating modes. Invoked in "point" mode the simulator calculates the specific attenuation for a point at a given altitude, for a given set of atmospheric conditions. When invoked in "path" mode, the simulator traces the ray path, and then invokes itself in "point" mode to calculate the cumulative propagation impairments for each of the internal models.

Parameters and calculated values are passed to and from the simulator using a large C language structure. This was intended to facilitate the addition of parameters as required, and proved to be useful in the latter stages of development.

2 Propagation Loss Models

The propagation loss models mostly fall into two categories, gaseous resonance absorption losses and rain or cloud droplet scattering losses. Gaseous losses exhibit dependencies upon temperature, pressure and water vapour density, while cloud scattering losses exhibit a temperature dependency.

Therefore an atmospheric model is required to find the temperature, pressure and water vapour density at any given altitude to provide parameters for the loss models.

3 The Atmospheric Model

The atmospheric model is divided into three components, which respectively calculate the variations of temperature, pressure and water vapour density against altitude.

The temperature and pressure models at this time conform to the basic ICAO ISA atmospheric model. Absolute temperature T [K] is approximated as a piecewise linear function of geopotential altitude h_g [km], defined as:

$$\begin{aligned} T &= 288.16 - 6.5h_g \quad \text{for } h_g \leq 11 \\ T &= 288.16 \quad \text{for } 11 < h_g \leq 25 \end{aligned}$$

$$T = 216.66 + 3.0(h_g - 25.0) \quad \text{for } h_g > 25$$

The temperature model was derived from [3], and published ICAO tables. Figure 1 compares the calculated ISA model against the ISA tabulated data points.

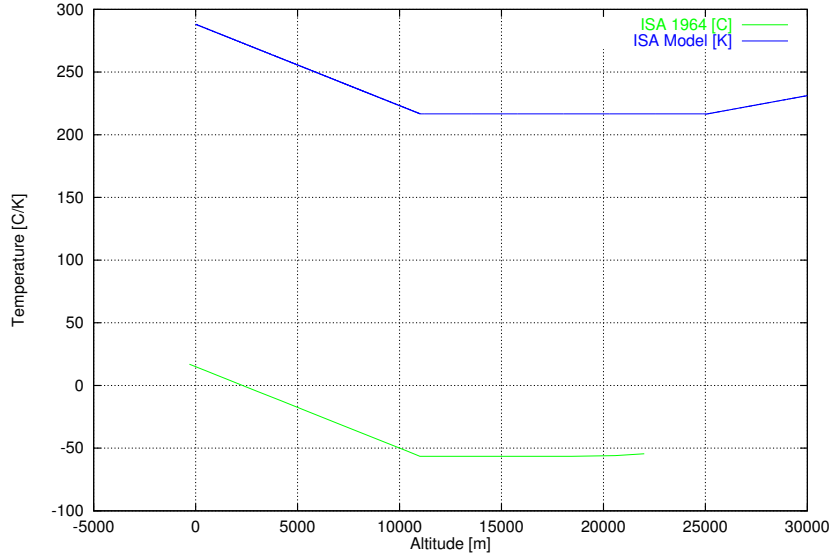


Figure 1: Calibration Curve for ISA Temperature Profile Model. Model is in Kelvins.

The model for pressure [hPa] variation with altitude is more complex than the temperature model, and uses the previously computed temperature variation with altitude:

$$p = 1013.25 \left(\frac{T}{288.16} \right)^\alpha \quad \text{for } h_g \leq 11$$

$$p = 226.128 e^{-\beta (h_g - 11)} \quad \text{for } 11 < h_g \leq 25$$

$$p = 24.886 \left(\frac{216.66}{T} \right)^\gamma \quad \text{for } h_g > 25$$

Where $\alpha = 5.256122$, $\beta = 0.157499$ and $\gamma = 11.388265$. The pressure model was also derived from [3], and published ICAO tables¹. The water vapour density model was produced by fitting a function to an empirical dataset. The resulting expression relating water vapour density to its sea level value and geopotential altitude is:

¹ Expressions 5.41 through 5.43 of [3] require adjustment to fit the published data. Blake derives these models from Minzner, Ripley and Condron, 1958. , with the expression for altitudes between 11 and 25 km altered to achieve a better fit to the ICAO dataset. Figure 2 compares the calculated ISA model against the ISA tabulated data points.

$$\rho_{WV} = \rho_{WV\ SL} e^{-\frac{1}{2}\left(\frac{2}{3}h_g\right)^{\frac{5}{2}}} \text{ for } h_g \leq 15$$

At altitudes above 15 km the value of geopotential altitude in the exponential is fixed at 15 km. The dataset was produced by Sissenwine, Grantham and Salmella in 1968 and cited in [3]. Figure 3 compares the calculated model with the empirical dataset, the model is conservative at higher altitudes thereby yielding slightly higher water vapour loss than the empirical data would yield.

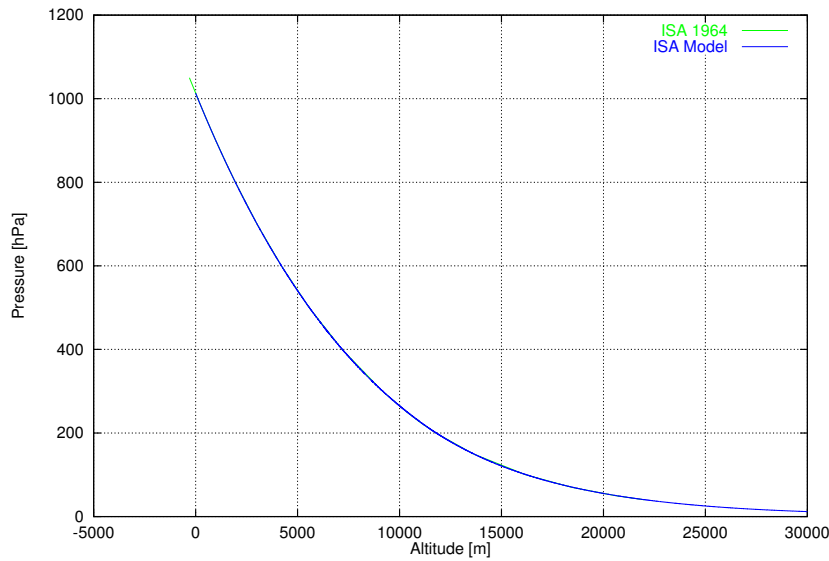


Figure 2: Calibration Curve for ISA Pressure Profile Model.

The TROPPO simulator has provisions to vary initial sea level temperature, pressure and water vapour density values, however these are disabled in the current implementation and standard values are assumed.

4 The Water Vapour Absorption Model

Losses produced in the 10-100 GHz bands by water vapour resonances occur at the single 22.235 GHz line, and as a result of the residual tails of a number of resonance lines above 100 GHz. These effects are extensively described in the literature. The TROPPO simulator implements a variant of the Liebe equations, summarised in [3], using the Van Vleck-Weisskopf function for line broadening effects.

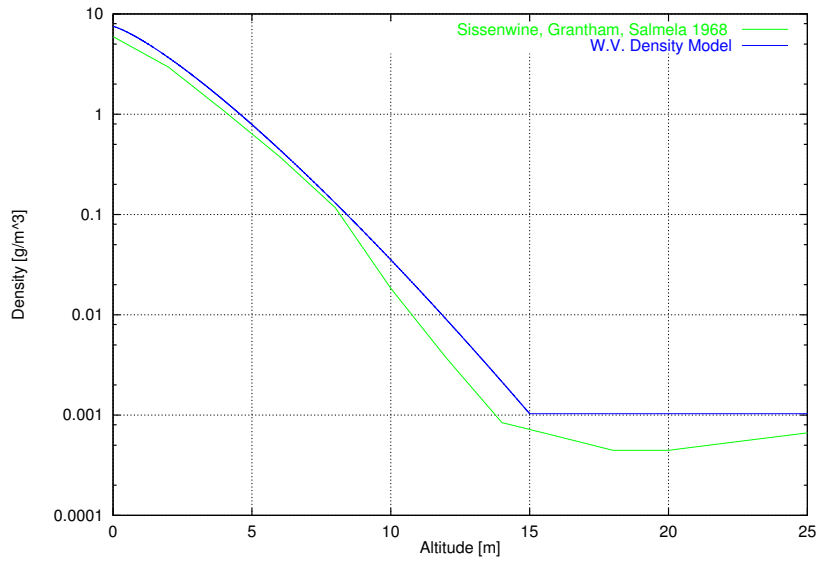


Figure 3: Calibration Curve for Water Vapour Density Profile Model.

Computation of the 22.235 GHz water vapour resonance loss rate [dB/km] is performed in several steps, starting with previously evaluated results for pressure, temperature and water vapour density, for a given altitude and frequency.

The water vapour partial pressure is computed from the water vapour density:

$$p_T = 0.75 p$$

$$p_{WV} = \rho_{WV} \frac{T}{288.75}$$

Where pressures are in [torr].

The Van Vleck broadening factor is computed for the frequency, temperature and water vapour partial pressure specified, in two steps:

$$\Delta f = 17.99 \times 10^{-3} \times \left(p_{WV} \frac{300}{T} + 0.20846(p_T - p_{WV}) \left(\frac{300}{T} \right)^{0.63} \right)$$

$$F = \frac{f}{f_r} \left(\frac{\Delta f}{(f_r - f)^2 + (\Delta f)^2} + \frac{\Delta f}{(f_r + f)^2 + (\Delta f)^2} \right)$$

The loss rate in dB/km is computed, using the Van Vleck broadening factor and the Liebe equation:

$$\gamma_{22} = 2.53397 \times 10^{-3} f p_{WV} \left(\frac{300}{T} \right)^{\frac{7}{2}} e^{2.144 \left(1 - \frac{300}{T} \right) F}$$

The computation of the residual 100 GHz line losses is simpler, and uses the values of water vapour density, pressure, temperature and frequency:

$$\gamma_{100} = 0.4 \frac{\rho_{WV}}{\rho_{WV SL}} \frac{p_T}{p_{SL}} \left(\frac{T_{SL}}{T} \right)^{\frac{5}{2}} \left(\frac{f}{f_r} \right)^2$$

The resulting loss contributions for the 22.235 GHz line and residuals from the 100 GHz lines are then summed to yield the total water vapour loss for the given atmospheric conditions.

$$\gamma_{H_2O} = \gamma_{22} + \gamma_{100} \text{ [dB/km]}$$

5 The Oxygen Absorption Model

The computation of losses resulting from the cluster of oxygen resonance lines grouped at 60 GHz is more complex than the water vapour loss, but similar in basic form. The implementation is based on the Meeks and Lilley model, with a refined nonresonant component model by Reber, Mitchell and Carter (RMC), and is derived from the original Van Vleck model [3]. The resonances occur in pairs for odd rotational quantum numbers up to $N = 45$, producing 46 discrete lines between 48.453 and 118.7503 GHz, in addition to a nonresonant component. The Van Vleck-Weisskopf model is employed for the resonant components, and the RMC model for the nonresonant contribution.

The algorithm has several steps, initially the RMC model parameters are calculated to produce the Δf term, using previously computed values of pressure and temperature. A loop is then employed to sum the resonant and nonresonant contributions from each oxygen line.

The RMC model is implemented as:

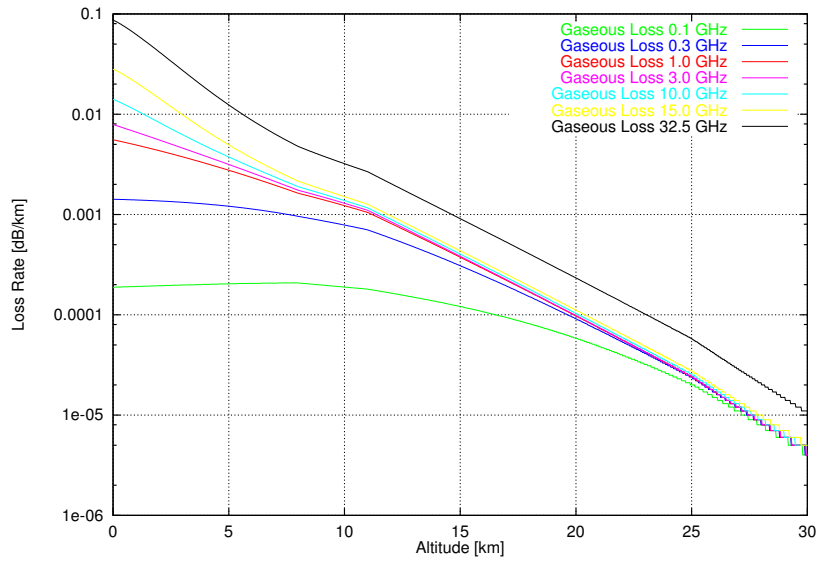


Figure 4: Gaseous loss rate model, parametrised for a range of frequencies (cf Blake 5-11 [3]).

$$\Delta f(h_g) = \frac{p}{p_{SL}} \frac{T_{SL}}{T} g(h_g)$$

where:

$$g(h_g) = 0.640 \quad \text{for } 0 < h_g \leq 8$$

$$g(h_g) = 0.640 + 0.04218 (h_g - 8) \\ \text{for } 8 < h_g \leq 25$$

$$g(h_g) = 1.357 \quad \text{for } 25 < h_g$$

The contributions for each line are then computed, with the frequency value indexed in a table by loop count. The computation is done in two steps, first finding the terms for the non-resonant contribution, which are the line broadening factor and the weighting factor:

$$F_0 = \frac{\Delta f}{f^2 + (\Delta f)^2}$$

$$\mu_{N0}^2 = \frac{2(N^2 + N + 1)(2N + 1)}{N(N + 1)}$$

The resonant terms are then:

$$F_{N\pm} = \frac{\Delta f}{(f_{N\pm} - f)^2 + (\Delta f)^2} + \frac{\Delta f}{(f_{N\pm} + f)^2 + (\Delta f)^2}$$

$$\mu_{N+}^2 = \frac{N(2N + 3)}{N + 1}$$

$$\mu_{N-}^2 = \frac{(N + 1)(2N - 1)}{N}$$

The resonant and nonresonant contributions are then combined to produce the total contribution for the line, and the contributions for all lines are summed:

$$\gamma_{O_2} = 2.0058 \frac{p_T}{T^3} f^2 \times \sum_N (\mu_{N+}^2 F_{N+} + \mu_{N-}^2 F_{N-} + \mu_{N0}^2 F_0) e^{-\frac{2.06844N(N+1)}{T}}$$

[dB/km]

The resulting model output is in close agreement with the results of Blake. The parametrised dependency of loss rate in dB/km against altitude in Blake Figure 5-11 was simulated to confirm the accuracy of model. This is shown in Figure 4.

Figure 5 is a plot of the frequency dependency of loss rate parametrised for a range of relevant altitudes, covering the range from 10 to 120 GHz. The fine structure of the 60 GHz absorption region is pronounced, as is the altitude dependency of the water vapour absorption line. The fine structure of the oxygen resonances is plotted in Figure 6, on a linear rather than logarithmic frequency scale.

6 The Lens Effect Loss Model

Lens effect losses occur due to refraction, where the pathlength covered by a beam of finite angular height varies across the height of the beam. As a result for some geometries the beam

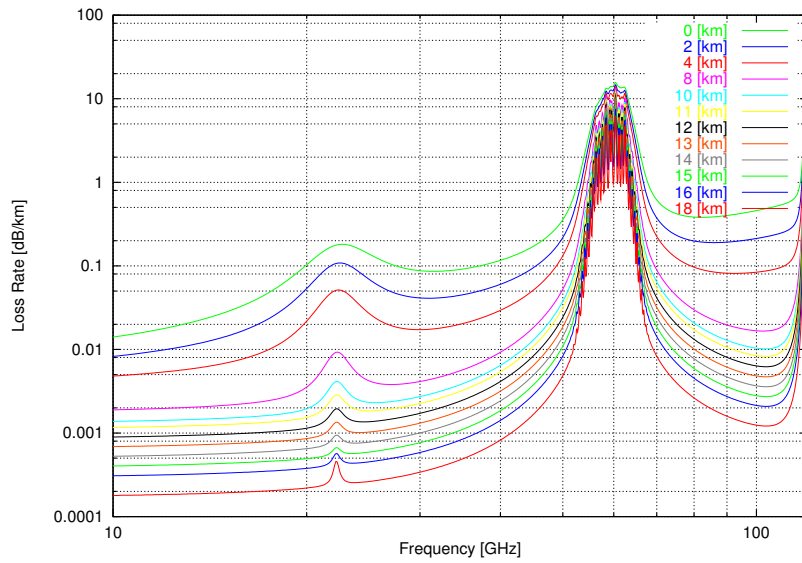


Figure 5: Gaseous Loss vs Frequency using the combined Van Vleck, Liege and Blake models, assuming an ISA atmosphere and water vapour density of $7.5 [g/m^3]$. Frequency is logarithmic between 10 and 120 [GHz].

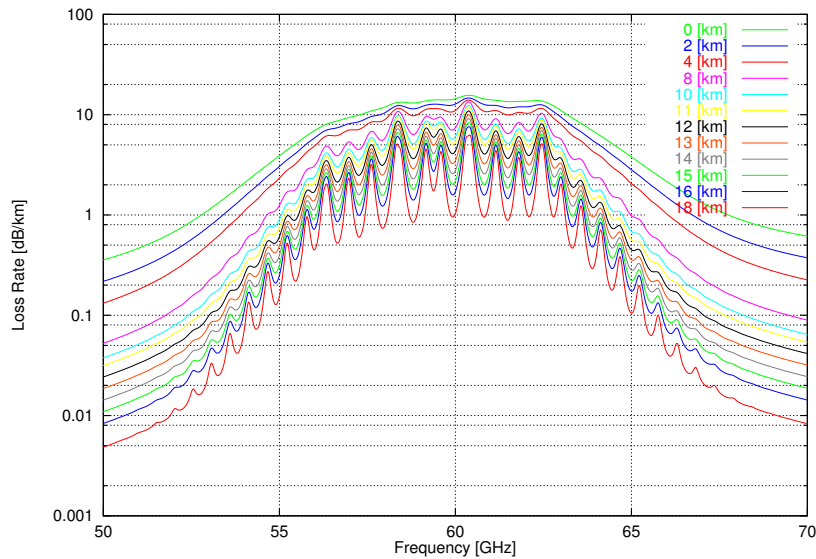


Figure 6: Fine structure of gaseous loss vs frequency dependency using the combined Van Vleck, Liege and Blake models, assuming an ISA atmosphere and water vapour density of $7.5 [g/m^3]$. Frequency scale is linear between 50 and 70 [GHz].

is defocussed and this appears as a loss in received power.

The model used in [3] was adopted, but its implementation was unconventional. The classical approach is to raytrace the paths corresponding the upper and lower vertical extents (eg -3 dB mainlobe width) and employ these to evaluate the loss incurred. Our strategy exploited the BVP shooting method, inserting the initial and final BVP shots into the loss model. In this manner no penalty is incurred in compute effort. Because the launch angles of the initial and final BVP shots are of a similar order of magnitude in size to the beamwidth, the error is negligible in magnitude. The equation for calculating the loss is:

$$L_{LE} = 10 \log_{10}\left(\frac{\epsilon}{\delta R}\right) [dB]$$

Where ϵ is the difference in launch angles, δ the difference in final beam positions, and R the mean pathlength. The results were found to be in close agreement with Blake's results.

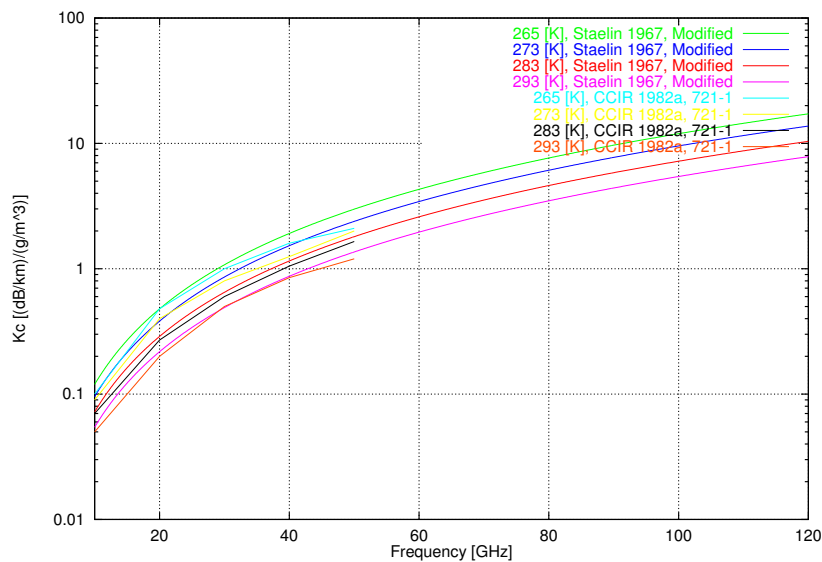


Figure 7: Modified Staelin cloud droplet loss model, compared with CCIR 1982a dataset (721-1).

7 The Cloud Scattering Loss Model

Losses due to Rayleigh scattering effects in cloud or fog are modelled using a modified version of the Staelin (1967) model [2]². The Staelin model was adjusted to provide results which better fit the CCIR 1982a Water Droplet Attenuation Coefficient plots [1].

The revised Staelin model is used to calculate the density specific attenuation in for a given frequency and temperature:

$$K_c = 12.8889 \times 10^{-3} \times \log_{10}(e) 10^{0.0122 (292.0 - T) - 1} f^2 [(dB/km)/(g/m^3)]$$

The density specific attenuation is then used to calculate the specific attenuation for the given conditions, and this is used to find the loss:

$$A_c = K_c \rho_c [dB/km], \quad L_c = A_c d [dB]$$

Figure 7 plots the modified Staelin cloud loss model against the CCIR 1982a model. The results are in close agreement and at no time does the modified Staelin model underestimate loss, against the CCIR model.

For path calculations the cloud scattering loss is calculated for 1 km increments and summed, when the ray is within a cloud layer. The TROPPO simulator at this time has provisions for two discrete cloud layers with unique parameters. A cloud layer is specified by its base and height in km, coverage as a fraction (typically specified by meteorologists in eighth's of coverage, eg 8/8 for full coverage and 1/8 for 12.5% coverage), and by the cloud density. Density may be specified explicitly where known, or estimated using a internal algorithm. The estimation algorithm uses a cloud type and grade specifier to look up a representative value of density from a table. The table was compiled from density data in [3], [4], [2] and [1], and covers all three cloud etages. Cloud types recognised are *Stratus*, *Cumulus*, *StratoCumulus*, *NimboStratus*, *CumuloNimbus*, *AltoStratus*, *AltoCumulus*, *Cirrus*, *CirroStratus* and *CirroCumulus*, graded as *light*, *medium* and *heavy*³.

² The Staelin model cited in [2], Eq 5.21 contains a typographical error, and is unusable without proper adjustment.

³ Given the diversity of sources used, and the highly variable density in any given cloud type, the accuracy of the estimation may be under some conditions modest. For a highly accurate simulation the density should be specified explicitly.

8 The Rain Scattering Loss Model

The loss model for scattering due to rain drops is based upon the very widely used empirical model by Olsen and Rogers, as cited in [3], [4], [2] and [1], using the Rice exponential model for rain rate variation with altitude, and the Rivers coefficient and exponent formulas, as cited in [3]. The Olsen and Rogers model is of the form:

$$A_r = \alpha(f) R^{\beta(f)}$$

R is the rain rate in mm/hr, the coefficient α and exponent β are defined as:

$$\alpha(f) = \frac{3.1 \times 10^{-5} f^2 \left(1 + \frac{f^2}{f_1^2}\right)^{\frac{1}{2}}}{\left(1 + \frac{f^2}{f_2^2}\right)^{\frac{1}{2}} \left(1 + \frac{f^2}{f_3^2}\right)^{\frac{1}{2}} \left(1 + \frac{f^2}{f_4^2}\right)^{\frac{1}{2}}}$$

$$f_1 = 3.0, f_2 = 35.0, f_3 = 50.0, f_4 = 110.0 \text{ [GHz]}$$

$$\beta(f) = 1.30 + 0.0372 \left(1 - \left(1 + x^2\right)^{\frac{1}{2}}\right),$$

$$x = \frac{\log_{10}\left(\frac{f}{10.0}\right)}{0.06}$$

The Rice model for rain rate variation with altitude is a simple scale height model:

$$r(h) = r_{SL} e^{-\left(\frac{h}{h_s}\right)^2}$$

The TROPPO loss model is invoked with a rain rate at sea level, altitude, scale height and frequency, and returns the loss rate in dB/km for these conditions.

The implementation of the Olsen and Rogers model demonstrates good agreement with published CCIR data [2], and within the frequency range of interest also with [5].

Unlike the cloud model, TROPPO supports only a single rain layer model. The rain loss is computed for 1 km increments of ray path length when within rain, and then summed to yield a total rain loss for the path.

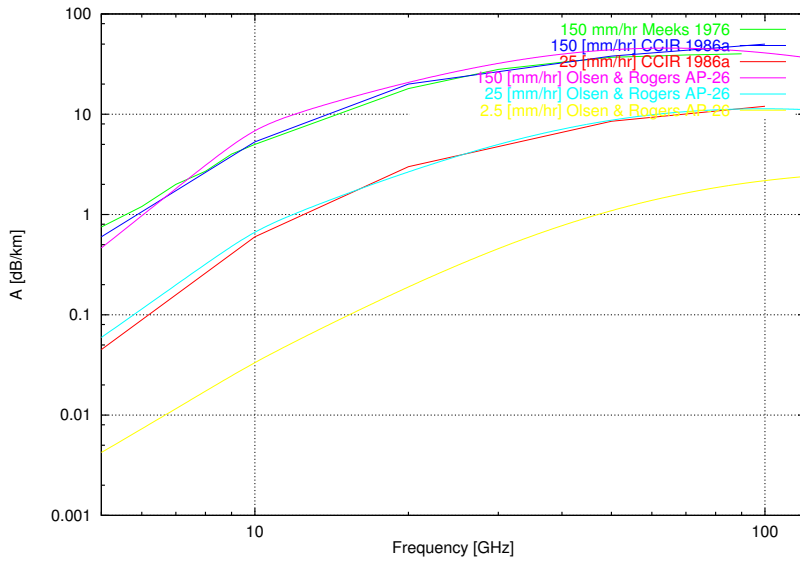


Figure 8: Olsen and Rogers rain loss model output, compared with Meeks 1976 and CCIR 1986a loss data.

9 The Refractive Model

The requirement for accurate modelling of cloud and rain losses introduced the need for ray path tracing of reasonable accuracy. Geometries with shallow depression or elevation angles experience a large error in cloud or rain penetration distance with even a modest error in ray path elevation. The Schelleng, Burrows and Ferrell (SBF) or effective earth radius model [3], [4] was explored and found to produce unacceptable results. Modified variants of the SBF model were also unsatisfactory since none were able to address the large variations in refractive index between the lower troposphere and stratosphere.

The refractive properties of the atmosphere were modelled with the widely used CRPL exponential model using a sea level refractivity of 313 and scale height of 6.95 km. The nonlinear second order differential equation describing the ray path is:

$$\frac{\partial^2 y}{\partial x^2} = \left(1 + \left(\frac{\partial y}{\partial x} \right)^2 \right) \left(\frac{1}{R} + \frac{\partial}{\partial y} \log(n(y)) \right)$$

An attempt was made to solve the equation analytically, using a nine term series to approximate the exponential as this removed the analytical difficulties with the exponential. This was also

found to be cumbersome and abandoned⁴.

The specific problem of interest is finding the ray path which connects a pair of stations each with a known height above the earth's surface, and separated by a known distance along the earth's surface. This is a classical Boundary Value Problem (BVP), complicated by the nonlinearity of the ordinary differential equation describing the curve.

The numerical technique chosen to solve this BVP was the shooting method [6], [7], [8], employing a numerical integration algorithm to solve the ray path Initial Value Problem (IVP) for a known initial height and variable ray launch angle.

Two techniques were employed for the IVP integration. Initially a second order predictor-corrector algorithm was used [6], [7], this yielded satisfactory results for modest increment sizes of the order of a kilometre, but its speed performance was not satisfactory for traces with aggregate lengths of the order of hundreds of kilometres.

A more elaborate fourth order multistep technique by Wallace and Gupta was then implemented and tested [9], achieving an order of magnitude better speed performance with increments of 20 km size still yielding suitable accuracy. A simple linear interpolation was employed to provide the intermediate 1 km sample points between the computed 20 km intervals, this still provided a less than 0.1% error against the second order method.

Testing indicated that the fourth order method would require further refinement for shorter distance ray paths, in the interest of expediency the TROPPO simulator uses the second order method for distances up to 150 km, and the fourth order method for all greater distances.

The BVP is solved using a secant method for convergence, which under best case conditions achieves a final height error of the order of 0.05% in 3 iterations. During the computation the values of initial and final launch angles and heights are saved to provide values for the lense effect loss calculation.

The output from the computation is an array of height points at 1 km intervals.

10 Path Loss, SNR and Capacity

The calculation of path loss employs the classical Friis model [10]. The integrated pathlength is employed, together with configurable parameters for the system design. These are transmitter EIRP in dBW, centre frequency in GHz, link bandwidth in GHz, receive antenna gain in dBi,

⁴ The Wolfram Mathematica package was used in this attempt but failed to complete the second integration after several days of computation. At this point it was decided to use numerical methods.

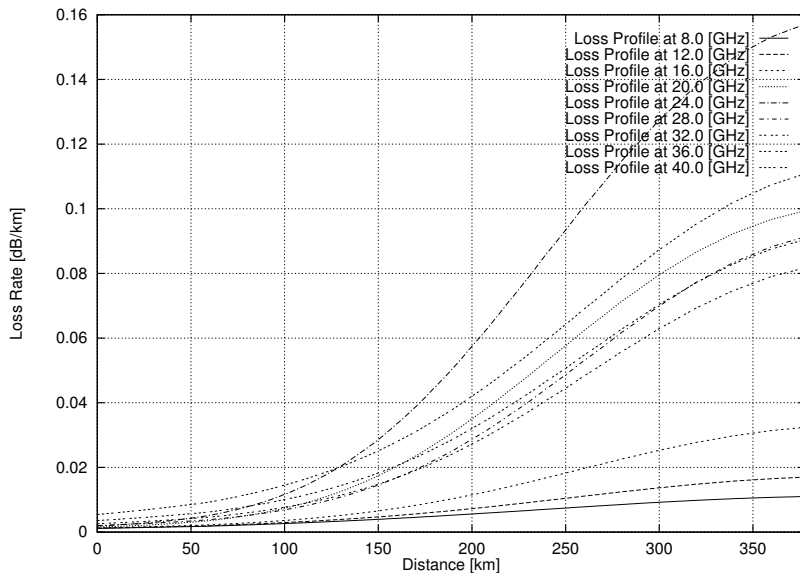


Figure 9: Gaseous loss profiles for station altitudes of 11.0 [km] and 0.2 [km] respectively, separated by 380 [km].

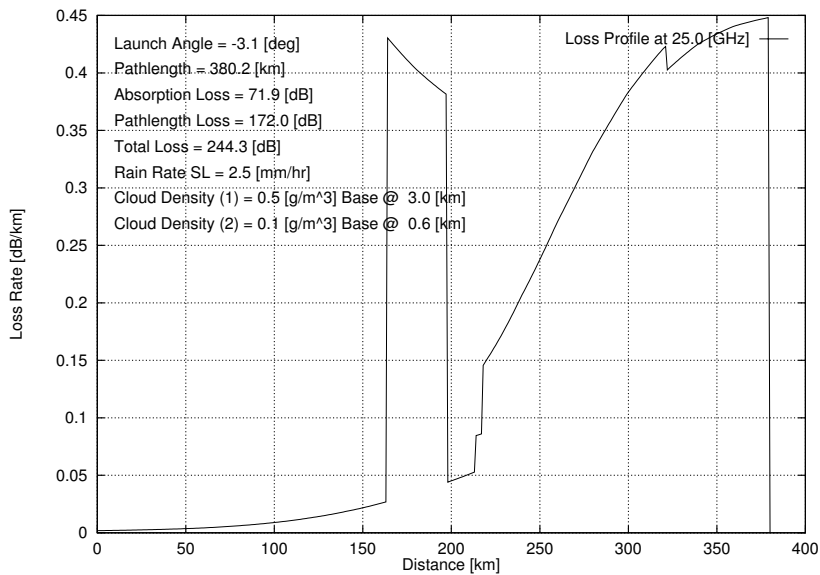


Figure 10: Aggregate loss profile for station altitudes of 11.0 [km] and 0.2 [km] respectively, separated by 380 [km], at 25 [GHz]. The weather model assumes two cloud layers and rain.

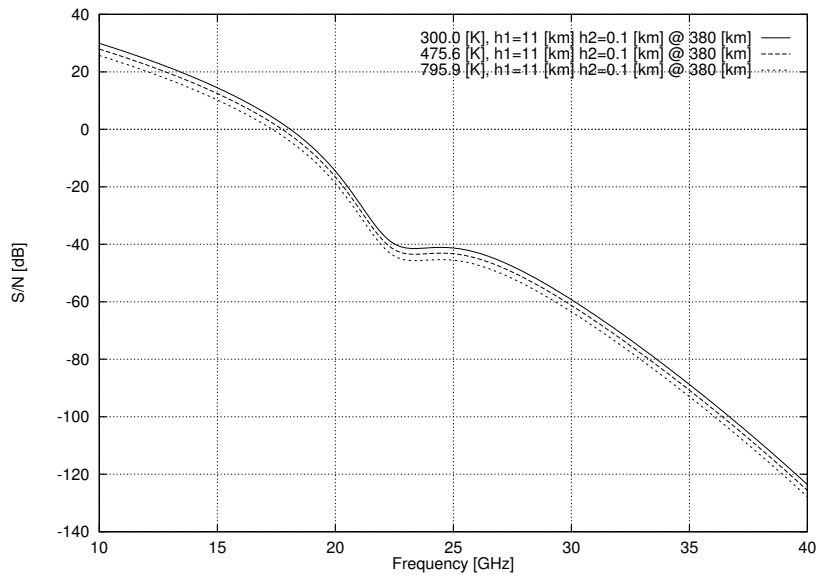


Figure 11: Frequency dependency of SNR, for station altitudes of 11.0 [km] and 0.1 [km], respectively, separated by 380 [km], assuming previous weather environment. EIRP is assumed to be 68.8 [dBW], fractional bandwidth 1% of carrier frequency, and system noise temperatures spanning 300 to 795.9 [K].

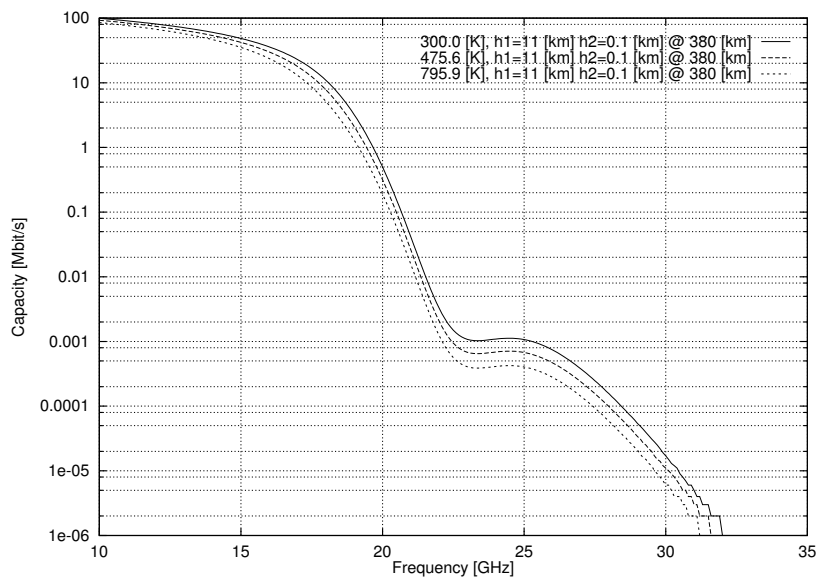


Figure 12: Frequency dependency of link channel capacity, for the conditions in Fig.11.

LNA gain in dB and system noise temperature.

For these parameters the simulator will calculate the SNR in dB at the receiver output, and the Shannon channel capacity in Mbit/s for these conditions. The choice of Shannon channel capacity was intentional, so as to provide a wholly general measure of digital throughput, without the encumbrance of a specific modulation scheme.

11 Combined Simulations

The TROPPO simulator can provide a wide range of simulations. The simplest are height profiles and loss profiles for given initial conditions. Height profiles can be used to check for terrain clearance, and clearance above cloud or rain layers. The loss profile for a ray path can be exceptionally useful, since it directly illustrates the lossiness of the transmission environment, and the pronounced sensitivity of loss to the ray path geometry. An example for pure gaseous loss conditions, over a range of frequencies, is depicted in Figure 9. Applying two layers of cloud, and rain, to a similar ray path geometry at a single frequency of 25 GHz yields the plot in Figure 10. This plot clearly shows the variations in lossiness for the cloud layers, with altitude, as well as the underlying gaseous losses.

Another interesting application is the use of TROPPO to analyse achievable SNR and channel capacity for a range of transmission environments, geometries, link parameters and frequencies.

Figures 11. and 12. respectively illustrate the frequency and system noise temperature dependencies of SNR and channel capacity for a link between two stations, one at 11 km and the other at 100 metres, separated by 380 km, in the weather environment of Figure 10. The EIRP is fixed at 68.8 dBW and the receiver bandwidth is 1% of the carrier frequency.

Other types of analysis have been performed with TROPPO. An example is that of the dependency of total gaseous and weather related loss, parametrised by frequency, for fixed station elevations and increasing distance between the station. The rapid increase in loss rate and total loss is very pronounced for a pair of airborne stations above the weather layer, once the ray path dips into cloud and rain.

12 Conclusions

We have developed and tested a general purpose numerical simulation tool for microwave propagation between stations of arbitrary altitude in the troposphere and stratosphere. Several existing models for atmospheric temperature, pressure and water vapour density, gaseous

oxygen and water vapour losses, cloud losses and rain losses were adapted, and modified where appropriate to better fit empirical data and semi-empirical models. The accuracy of these models has been confirmed by comparison with published data.

The simulation tool has proven to be useful for the analysis of propagation losses under a wide range of conditions, especially under conditions which are not well addressed by the large base of existing satellite and radar propagation literature.

The simulator can be used as a dedicated analytical tool, or incorporated in other more complex simulations, for areas such as high speed mobile communications, satellite communications, airborne radar propagation and electromagnetic signature analysis.

Future extensions to the simulator are intended to include a Graphical User Interface, additional loss models and fast table driven routines for the solution of the ray tracing boundary value problem.

13 Background

Professor C.S Wallace, *FACM*, *FACS* provided the second and first order IVP algorithms, and the secant based BVP shooting algorithm, as well as implementation and performance enhancements.

References

- [1] Ippolito L.J. *Propagation Effects Handbook for Satellite Systems Design, A Summary of Propagation Impairments on 10 to 100 GHz Satellite Links with Techniques for System Design* , NASA Reference Publication 1082 (04), 4th Edition, 1989, NASA Scientific and Technical Information Division
- [2] Flock W.L. *Propagation Effects on Satellite Systems at Frequencies Below 10 GHz, A Handbook for Satellite Systems Design* , NASA Reference Publication 1108 (02), 2nd Edition, 1987, NASA Scientific and Technical Information Division
- [3] Blake L.V. *Radar Range-Performance Analysis* , Lexington Books, 1980, Ma.
- [4] Blake L.V. "Prediction of Radar Range" in Skolnik M.I. (Ed) *Radar Handbook* Second Edition, McGraw Hill, 1991.
- [5] Meeks M.L. *Radar Propagation at Low Altitudes* , Artech House. 1982. Ma.

-
- [6] Maron M.J. and Lopez R.J. *Numerical Analysis: A Practical Approach* , Section 8. Third Edition. Wadsworth. 1990. Belmont. Ca.
- [7] Kincaid D.R. and Cheney E.W. *Numerical Analysis* , Ch.8. Wadsworth. 1991. Belmont. Ca.
- [8] Gerald C.F. and Wheatley P.O. *Applied Numerical Analysis* , Third Edition. Ch.6. Addison-Wesley. 1984.
- [9] Wallace C.S. and Gupta G.K. "General Linear Multistep Methods to Solve Ordinary Differential Equations" *The Australian Comp. Journal*. Vol.5, No.2, May, 1973.
- [10] Kraus J.D. *Antennas* Second Edition, McGraw Hill, 1988.